First results with the IOTA3 imaging interferometer: The spectroscopic binaries λ Vir and WR 140

J. D. Monnier[1], W. A. Traub[2], F. P. Schloerb[5], R. Millan-Gabet[3], J.-P. Berger[4], E. Pedretti[2], N. P. Carleton[2], S. Kraus[5], A. Ahearn[2], M. Brewer[5], C. Coldwell[2], P. Haguenauer[8], P. Kern [4], P. Labeye[10], M. G. Lacasse[2], L. Lagny[4], F. Malbet[4], D. Malin[5], P. Maymounkov[2], S. Morel[6], C. Papaliolios[2], K. Perraut[4], M. Pearlman[2], I. L. Porro[7], S. Ragland[2], I. Schanen[9], K. Souccar[5], G. Torres[2], and G. Wallace[5]

Received _____; accepted _____

[1]monnier@umich.edu: University of Michigan Astronomy Department, 941 Dennison Bldg, Ann Arbor, MI 48109-1090, USA.

[2]Harvard-Smithsonian Center for Astrophysics, 60 Garden St, Cambridge, MA, 02138, USA

[3]Michelson Science Center, California Institute of Technology, Pasadena, CA

[4]Laboratoire d'Astrophysique de Grenoble, 414 Rue de la Piscine 38400 Saint Martin d'Heres, France

[5]University of Massachusetts, Amherst

[6]European Southern Observatory, Germany

[7]Massachusetts Institute of Technology, Cambridge, MA

[8]Alcatel Space Industries, Cannes, France

[9]IMEP-INPG, Grenoble, France

[10]LETI-CEA, Grenoble, France

ABSTRACT

We report the first spatially-resolved observations of the spectroscopic binaries λ Vir and WR 140, which includes the debut of aperture-synthesis imaging with the upgraded three-telescope IOTA interferometer. Using a new integrated optics beam combiner capable of precise closure phase measurement, short observations were sufficient to extract the angular separation of each binary system and the component brightness ratio. Most notably, the underlying binary in the prototypical colliding-wind source WR 140 (WC7 + O4/5) was found to have a separation of $\sim$13 milli-arcseconds with a position angle consistent with the images of the 2001 dust shell ejection only if the Wolf-Rayet star is fainter than the O star at 1.65μm. We also highlight λ Vir whose peculiar stellar properties of the Am star components will permit direct testing of current theories of tidal evolution when the full orbit is determined.

Subject headings: instrumentation: interferometers – techniques: interferometric – stars: binaries: spectroscopic – stars: individual (WR 140, λ Vir),

1. Introduction

Only two optical (visible and infrared) interferometers have published results combining three or more separated telescopes, the Cambridge Optical Aperture Synthesis Telescope (COAST, Baldwin et al. 1996) and the Navy Prototype Optical Interferometer (NPOI, Benson et al. 1997). Combining more than two telescopes is crucial in order to measure the *closure phase* (CP), a phase quantity that is uncorrupted by atmospheric turbulence and necessary for image reconstruction in "very long baseline interferometry" (Jennison 1958; Monnier 2000); indeed, closure phase lies at the heart of so-called "self-calibration"

techniques widely used in the radio (e.g., Readhead et al. 1980; Cornwell & Wilkinson 1981).

The Infrared-Optical Telescope Array (IOTA) became the third optical interferometer to measure closure phases on U.T. 2002Feb23 (Traub et al. 2003). IOTA has much greater near-infrared sensitivity (demonstrated H mag 7) than the other imaging arrays, allowing new observational programs including imaging of young stellar objects, mass determinations of low-mass binaries, and mapping photospheric surface structures of red giants.

In this Letter, we present the first scientific results of the new three-telescope IOTA interferometer, with the new integrated-optics combiner IONIC3 (Berger et al. 2001) for precise measurements of visibility amplitudes and closure phases. The powerful combination of closure phases and visibilities at three simultaneous baselines allows binary stars to be resolved and characterized in a few hours rather than a few nights. After describing the novel interferometric instrumentation used for this work, we present the first resolved observations for the A-star binary λ Vir and colliding wind system WR 140 and briefly discuss the significance of our findings. Here we alert the astronomical community to the need for radial velocity follow-up of these specific sources as well as to the new research opportunities available with the upgraded IOTA3 interferometer.

2. Observations

All the data presented were obtained using the IOTA (Infrared-Optical Telescope Array) interferometer (Traub et al. 2003), a long baseline interferometer which operates at visible and near-infrared wavelengths. IOTA is operated by a consortium of institutions, most notably the Smithsonian Astrophysical Observatory and the University of Massachusetts at Amherst. The 0.45-m telescopes are movable among 17 stations along 2 orthogonal linear

arms (telescopes A & C can move along the 35-m northeastern arm, while Telescope B moves along the 15-m southeastern arm), allowing an aperture 15m×35m to be synthesized (corresponding to an angular resolution of ∼5×12 milliarcseconds at 1.65μm). IOTA is one of the most established optical interferometers in the world (see Monnier 2003, for a recent review), contributing key observations to published papers covering a range of topics: evolved star diameters (e.g., van Belle et al. 1996) and surface structure (Perrin et al. 1999), accretion disks around young stars (e.g., Millan-Gabet et al. 2001), Cepheid diameters (Kervella et al. 2001), and circumstellar dust shells (Monnier et al. 2004, submitted).

Capping a long development (e.g., Schloerb 1990), the third telescope ("C") was fully incorporated into IOTA on UT2002Feb23 and now allows visibilities on 3 baselines and one closure phase to be measured simultaneously. These initial observations used a prototype integrated optical (IO) combiner (e.g., Kern et al. 1997; Berger et al. 2001) which operated only with polarized light. The upgraded combiner IONIC3 corrected this deficiency in 2002 November, and all observations presented here were obtained in unpolarized light.

We only just introduce IONIC3 here and refer the interested reader to a recent description in Berger et al. (2003); an engineering paper with detailed description of the optical component and its performance is in preparation (Berger et al. 2004). Light from each telescope is focused into a dedicated single-mode fiber, and the three fibers are aligned using a silicon v-groove array mated to the planar waveguides on the IO device. The optical circuit acts to split the light from each fiber/telescope before recombining each telescope pair (AB,BC,AC) at 3 IO couplers. This "pair-wise" combination scheme leads to 6-interferometer channels (two for each baseline) and the fringes are detected using a sensitive HgCdTe (Rockwell PICNIC) detector (Pedretti et al. 2004a, submitted). Varying coupling efficiencies into the fibers cause the system visibilities to vary, however this effect can be directly calibrated using measurements of the IONIC3 (optical) transfer matrix

(which relates the six output channels to the three input channels for incoherent light).

The interference fringes are temporally-modulated on the detector by scanning piezo mirrors placed in two of the three beams of the interferometer. A typical single observation consisted of 200 scans obtained in ∼4 min, followed by calibration measurements of the background and single-telescope fluxes (important for characterizing the IO couplers). Target observations are interleaved with an identical sequence obtained on an unresolved or partially-resolved star, which serves to calibrate the interferometer's instrumental response and the effect of atmospheric seeing on the visibility amplitudes. The target and calibrator sources are typically separated on the sky by 5-10 degrees and are observed 10-20 minutes apart (although practices did vary for data presented here, which were collected during the early IOTA3 observing runs); these conditions ensure that the calibrator observations provide a good estimate of the instrument's transfer function.

The IONIC3 combiner itself operates with high efficiency (transmission $\gtrsim$50%) at 1.65μm, although operation can be pushed to longer wavelengths for stars where waveguide losses are tolerable. All the science targets presented here were observed using a standard H band filter ($\lambda_0 = 1.65\mu$m, $\Delta\lambda = 0.30\mu$m). Full observing information for our science targets can be found in Table 1, including dates of observation, interferometer configurations, and calibrator details; note that the calibrators are all nearly unresolved on our baselines and the size uncertainties do not significantly contribute to the calibration uncertainties. Figure 1 shows the (u,v)-coverage obtained during each epoch for each science target. In the next section, we discuss our preliminary analysis of these data and the techniques used to process raw data into calibrated squared-visibilities ($\mathcal{V}^2$) and closure phases (CP).

3. Analysis

Reduction of the IONIC3 visibility data was carried out using custom software similar in its main principles to that described by Coudé du Foresto et al. (1997, for the FLUOR experiment), developed using the *Interactive Data Language* (IDL). In short, we measure the power spectrum of each interferogram (proportional to the target $\mathcal{V}^2$), after correcting for intensity fluctuations and subtracting out bias terms from read noise, residual intensity fluctuations, and photon noise (e.g., Perrin 2003). We require that interferograms are detected for at least two of the three baselines in order to assure a good closure phase measurement; this condition is almost always met due our reliance on a realtime fringe "tracker" (discussed further below). Lastly, the data pipeline applies a correction for the variable flux ratios for each baseline by using a transfer matrix (e.g., Coudé du Foresto et al. 1997; Monnier 2001). We have studied our calibration accuracy by observing single stars of known size. Under the worst observing conditions (i.e., large gaps in time between measurements and large angular separations on the sky), we found a systematic error of $\Delta V^2 = 0.10$ (e.g., 5% error in visibility for unresolved sources) and have combined this error (in quadrature) with the statistical error of each observation for fitting purposes. While this level of calibration precision is similar to the performance of other optical interferometers and quite sufficient for our immediate scientific purposes, we do hope to achieve $\lesssim$1% visibility accuracy eventually since we are using single-mode fibers. We currently believe most of the systematic error is due to imperfect correction of coupling fluctuations into the fibers and significant effort is being expended to improve calibration.

In order to measure the closure phase, a fringe-tracking algorithm was applied in realtime while recording interferograms (Pedretti et al. 2004b, in preparation), ensuring that interference occurs simultaneously for all baselines. We followed the method of Baldwin et al. (1996) for calculating the complex triple amplitude in deriving the closure phase,

explicitly guaranteeing that the fringe frequencies for each triple-product determination also "close" ($\nu_{AB} + \nu_{BC} + \nu_{CA} = 0$). One calibration step of Baldwin et al. (1996) we do not need to apply is a photon-noise bias correction to the triple product (e.g., Wirnitzer 1985), which is only necessary for "all-in-one" combiners.

One additional calibration step with pair-wise combiners (such as IONIC3), unnecessary for "all-in-one" combiners, is determination of the instrumental offset for the closure phase. The instrumental closure phase of IONIC3 drifts less than 1 degree over many hours (in an unstabilized environment which can drift by >10 K during a night), owing to the miniature dimensions of the IO component. Also, chromaticity effects limit our absolute precision when the calibrator and source are not of the same spectral type due to different "effective wavelengths" when using the broadband H filter. Engineering tests indicate that the instrumental closure phase (Φ_{CP}) varies systematically by $\Delta\Phi_{CP} = 1.4 \pm 0.3$ degrees between a hot star (B8) and a cool star (M3) when using the broadband H filter. We minimize these errors through repeated calibration of our targets with calibrators of similar spectral type. In light of this, we have conservatively adopted a systematic error of $\Delta\Phi_{CP} = 0.75$ degs for the measurements presented here to represent the residual closure phase drifts and wavelength dependence. Refinement of our data pipeline should allow this error to be reduced in the near future by explicitly calibrating the wavelength-dependence with additional engineering data. Lastly, we established the sign of our closure phase (baseline triangle connecting telescopes A→B→C→A) using test measurements of Capella and Matar in comparison to published orbits (Hummel et al. 1994, 1998).

4. Results

With calibrated $\mathcal{V}^2$and closure phases for each target, a static binary star model (separation, position angle, brightness ratio) was fit to the data for each given epoch,

assuming the calibration errors given in the previous section and ignoring bandwidth-smearing effects. Table 2 contains the results of our fits based on a maximum-likelihood approach giving equal weights to the visibility data and closure phases. In addition, we have separately tabulated the the reduced χ^2 for the $\mathcal{V}^2$and closure phases data using our best-fitting model.

Explicitly, the probability of a given set of parameters was approximated by: Probability $\propto exp(-\frac{\chi^2_{\rm Vis^2}}{\rm minimum(\chi^2_{Vis^2})} - \frac{\chi^2_{\rm CP}}{\rm minimum(\chi^2_{CP})})$. This normalization is equivalent to increasing the data errors to force the χ^2/DOF= 1, and conservatively estimates errors in the context of an incomplete error model. The most probable values with 1-sigma errors bars (68.4% confidence interval) were calculated for each parameter (separation, positional angle, brightness ratio) by integrating over the other variables, a standard practice referred to as *marginalizing* over these variables.

Based on their brightness and color temperatures, the component stars of both binaries are expected to be small ($\lesssim$0.5 mas), and they have been assumed to be unresolved in these model fits; this assumption, as well as as neglecting bandwidth-smearing, may not remain valid if the data precision is improved significantly. The $\mathcal{V}^2$and closure phases for a subset of the data are shown in Figure 2 along with the best-fitting model prediction. These $\mathcal{V}^2$predictions have also been overlaid on their corresponding (u,v)-plane coverage in Figure 1. Not surprisingly, the closure phase data proved most important in constraining model parameters, because of the small systematic errors achieved compared to the visibilities.

The $\chi^2_{\rm Vis^2}$ is systematically below unity in Table 2, indicating we have over-estimated our systematic error contribution. In contrast, $\chi^2_{\rm CP}$ is larger than unity for all fits which indicates either the systematic error has been under-estimated or that the model is inappropriate. For λ Vir, which has a (short) $\sim$ 207 day period, we have confirmed by

inspecting the fit residuals that the large $\chi^2_{\rm CP}$ partly arises due to orbital motion of the binary during each "epoch" (worst for 2003Feb "epoch" which spanned 8 days). This is not an important effect for WR 140, and inspection of the closure phase data in Figure 2b reveals a few outlier data points with small error bars that dominate the $\chi^2_{\rm CP}$. With the larger dataset currently being collected, the visibility and closure phase data will be fit directly to the *orbital elements* at the same time as radial velocity (RV) information, as outlined in Hummel et al. (1998) and Boden et al. (1999).

The radio community developed interferometric imaging techniques known as hybrid mapping which are capable of reobtaining the lost individual phases (e.g., Haniff et al. 1987). As demonstrated by Baldwin et al. (1996), these methods can be applied successfully to optical interferometers as well. We present the first aperture synthesis images from IOTA in Figure 3, depicting λ Vir for all epochs. The images are constructed iteratively starting with zero initial phases and using the measured closure phase information for self-calibration. CLEAN deconvolution was applied using an elliptical Gaussian as clean beam. Full details of the image-making process for this source and for the well-studied binary Capella can be found in Kraus (2003). The presented maps are consistent with the binary parameters (separation and position angle) found through direct fitting, and demonstrate the imaging capability of the IOTA3+IONIC3 system, currently the most sensitive infrared imaging interferometer in the world.

For λ Vir, it is tempting to include here an orbital fit to the interferometry data using the existing spectroscopic information. We have carried out this exercise, but found the orbital inclination (the most important parameter not determined from the double-line RV orbit) to be poorly constrained by our temporal sampling: the first two epochs are close in time, while the third epoch is approximately 1/2 of an orbital period later (see Figure 3. New data taken at an intermediate orbital phase would strongly constrain the inclination,

hence the component masses, in this system; such an observing program is being pursued along with new RV data.

5. Discussion

The binary stars λ Vir and WR 140 have never been resolved before now. These systems were observed because they represent unique stellar systems whose properties can shed new light on rare and/or short-lived phases of stellar evolution.

λ Vir is a well-known spectroscopic binary with similar components of spectral type A. A double-lined orbit with a period of 207 days was derived by Stickland (1976). The stars exhibit the curious property that one is sharp-lined and the other broad-lined, which makes them easily distinguishable spectroscopically. Both are classified as metallic-lined stars (Abt 1961). Our interferometric observations with IOTA will allow a determination of the absolute properties of the components once the full orbit is established. The individual masses of the stars can be derived from a combination of spectroscopy (yielding lower limits to the mass, $M \sin^3 i$) and astrometry (providing the inclination angle). Furthermore, it is also possible to derive the distance to the system (orbital parallax) independently of the Hipparcos determination by combining the angular semimajor axis from interferometry with the projected semimajor axis in linear units from spectroscopy. The system brightness and the interferometric light ratio then give the individual luminosities in the near infrared. These properties can be compared directly against models of stellar evolution to derive the age of the system. The difference in the projected rotational velocities $v \sin i$ of the components is of special interest for these Am stars, and the stellar properties will allow us to test whether this is consistent with current theories of tidal evolution (Tassoul & Tassoul 1997; Zahn & Bouchet 1989, and references therein).

WR 140 is a prototypical colliding-wind binary source consisting of a Wolf-Rayet and an O4-5 star in a highly-eccentric ∼7.9 yr orbit, and it has been extensively studied in the radio, infrared, optical, ultra-violet, and X-rays (e.g., Moffat et al. 1987; Williams et al. 1990; White & Becker 1995). Dust emission has been observed to appear and fade in conjunction with periastron passage, explained by dust formation in the dense shock-compressed gas at the wind-wind interface (Williams et al. 1990; Usov 1991; Tuthill et al. 1999). This process was dramatically captured in a series of high-resolution near-infrared images by Monnier et al. (2002), who detected an eastward moving arc of dust consistent with the O-star being roughly east of the WR star at periastron. Because of the highly eccentric orbit, the O-star is predicted to be on (nearly) the opposite side of the WR star now as compared to periastron; this can be reconciled with the position angle determined here only if the WR star is fainter than the O-star at 1.65μm (as expected at visible wavelengths, e.g. Williams et al. 1990). As for λ Vir, we intend to combine future high-precision interferometer observations with new radial velocity data to derive component masses and a distance estimate, fundamental parameters for these systems needed for clear interpretation of data across the electromagnetic spectrum.

6. Conclusions

We have reported first scientific results from the IOTA3 interferometer, newly-resolved separation, position angle, and flux-ratio information for double-lined spectroscopic binary stars λ Vir and WR 140. Using a preliminary data reduction pipeline, calibration is sufficient for model-fitting and aperture-synthesis imaging using hybrid mapping techniques. New observations are being pursued in order to derive precise component masses and distance estimates by combining interferometric and radial velocity data. All the visibility and closure phases data here have been converted to the new FITS format for Optical

Interferometry data (OI-FITS) [11] and are available upon request.

The authors gratefully acknowledge support from NASA and SAO (for third telescope development) and the NSF (AST-0138303, for work on imaging with IOTA). EP was supported by a SAO Predoctoral fellowship, JDM by a Harvard-Smithsonian CfA fellowship, and RM-G, J-PB, and SR were partially supported through NASA Michelson Postdoctoral Fellowships. GT acknowledges partial support for this work from NASA's MASSIF SIM Key project (JPL grant 1240033). In addition, we wish to acknowledge useful contributions from B. Arezki, A. Delboulbe, C. Gil, S. Gluck, E. Laurent, R. B. Metcalf, and E. Tatulli. The IONIC3 instrument has been developed by LAOG and LETI in the context of the IONIC collaboration (LAOG, IMEP, LETI). The IONIC project is funded by the CNRS (France) and CNES (France). This research has made use of the SIMBAD database, operated at CDS, Strasbourg, France, and NASA's Astrophysics Data System Abstract Service. This publication makes use of data products from the Two Micron All Sky Survey, which is a joint project of the University of Massachusetts and the Infrared Processing and Analysis Center/California Institute of Technology, funded by the National Aeronautics and Space Administration and the National Science Foundation.

[11] http://www.mrao.cam.ac.uk/ jsy1001/exchange/

REFERENCES

Abt, H. A. 1961, ApJS, 6, 37

Baldwin, J. E., Beckett, M. G., Boysen, R. C., Burns, D., Buscher, D. F., Cox, G. C., Haniff, C. A., Mackay, C. D., Nightingale, N. S., Rogers, J., Scheuer, P. A. G., Scott, T. R., Tuthill, P. G., Warner, P. J., Wilson, D. M. A., & Wilson, R. W. 1996, A&A, 306, L13+

Benson, J. A., Hutter, D. J., Elias, N. M., Bowers, P. F., Johnston, K. J., Hajian, A. R., Armstrong, J. T., Mozurkewich, D., Pauls, T. A., Rickard, L. J., Hummel, C. A., White, N. M., Black, D., & Denison, C. S. 1997, AJ, 114, 1221

Berger, J., Haguenauer, P., Kern, P. Y., Rousselet-Perraut, K., Malbet, F., Gluck, S., Lagny, L., Schanen-Duport, I., Laurent, E., Delboulbe, A., Tatulli, E., Traub, W. A., Carleton, N., Millan-Gabet, R., Monnier, J. D., & Pedretti, E. 2003, in Interferometry for Optical Astronomy II. Edited by Wesley A. Traub . Proceedings of the SPIE, Volume 4838, pp. 1099-1106 (2003)., 1099–1106

Berger, J. P., Haguenauer, P., Kern, P., Perraut, K., Malbet, F., Schanen, I., Severi, M., Millan-Gabet, R., & Traub, W. 2001, A&A, 376, L31

Boden, A. F., Lane, B. F., Creech-Eakman, M. J., Colavita, M. M., Dumont, P. J., Gubler, J., Koresko, C. D., Kuchner, M. J., Kulkarni, S. R., Mobley, D. W., Pan, X. P., Shao, M., van Belle, G. T., Wallace, J. K., & Oppenheimer, B. R. 1999, ApJ, 527, 360

Cornwell, T. J. & Wilkinson, P. N. 1981, MNRAS, 196, 1067

Coudé du Foresto, V., Ridgway, S., & Mariotti, J.-M. 1997, A&AS, 121, 379

Haniff, C. A., Mackay, C. D., Titterington, D. J., Sivia, D., & Baldwin, J. E. 1987, Nature, 328, 694

Hummel, C. A., Armstrong, J. T., Quirrenbach, A., Buscher, D. F., Mozurkewich, D., Elias, N. M., & Wilson, R. E. 1994, AJ, 107, 1859

Hummel, C. A., Mozurkewich, D., Armstrong, J. T., Hajian, A. R., Elias, N. M., & Hutter, D. J. 1998, AJ, 116, 2536

Jennison, R. C. 1958, MNRAS, 118, 276+

Kern, P., Malbet, F., Schanen-Duport, I., & Benech, P. 1997, in Integrated Optics for Astronomical Interferometry, 195–+

Kervella, P., Coudé du Foresto, V., Perrin, G., Schöller, M., Traub, W. A., & Lacasse, M. G. 2001, A&A, 367, 876

Kraus, S. 2003, Master's thesis, University of Massachusetts, Amherst

Millan-Gabet, R., Schloerb, F. P., & Traub, W. A. 2001, ApJ, 546, 358

Moffat, A. F. J., Lamontagne, R., Williams, P. M., Horn, J., & Seggewiss, W. 1987, ApJ, 312, 807

Monnier, J. D. 2000, in Principles of Long Baseline Stellar Interferometry, 203–+

Monnier, J. D. 2001, PASP, 113, 639

—. 2003, Reports of Progress in Physics, 66, 789

Monnier, J. D., Tuthill, P. G., & Danchi, W. C. 2002, ApJ, 567, L137

Perrin, G. 2003, A&A, 398, 385

Perrin, G., Coudé du Foresto, V., Ridgway, S. T., Mennesson, B., Ruilier, C., Mariotti, J.-M., Traub, W. A., & Lacasse, M. G. 1999, A&A, 345, 221

Readhead, A. C. S., Walker, R. C., Pearson, T. J., & Cohen, M. H. 1980, Nature, 285, 137

Schloerb, F. P. 1990, in Amplitude and intensity spatial interferometry; Proceedings of the Meeting, Tucson, AZ, Feb. 14-16, 1990 (A91-30676 12-89). Bellingham, WA, Society of Photo-Optical Instrumentation Engineers, 1990, p. 154-165., 154–165

Stickland, D. J. 1976, in IAU Colloq. 32: Physics of Ap Stars, 701–+

Tassoul, M. & Tassoul, J. 1997, ApJ, 481, 363

Traub, W. A., Ahearn, A., Carleton, N. P., Berger, J., Brewer, M. K., Hofmann, K., Kern, P. Y., Lacasse, M. G., Malbet, F., Millan-Gabet, R., Monnier, J. D., Ohnaka, K., Pedretti, E., Ragland, S., Schloerb, F. P., Souccar, K., & Weigelt, G. 2003, in Interferometry for Optical Astronomy II. Edited by Wesley A. Traub. Proceedings of the SPIE, Volume 4838, pp. 45-52 (2003)., 45–52

Tuthill, P. G., Monnier, J. D., & Danchi, W. C. 1999, Nature, 398, 487

Usov, V. V. 1991, MNRAS, 252, 49

van Belle, G. T., Dyck, H. M., Benson, J. A., & Lacasse, M. G. 1996, AJ, 112, 2147

White, R. L. & Becker, R. H. 1995, ApJ, 451, 352+

Williams, P. M., van der Hucht, K. A., Pollock, A. M. T., Florkowski, D. R., van der Woerd, H., & Wamsteker, W. M. 1990, MNRAS, 243, 662

Wirnitzer, B. 1985, Optical Society of America Journal, 2, 14

Zahn, J.-P. & Bouchet, L. 1989, A&A, 223, 112

Table 1. Observing Log for λ Vir and WR 140

Date (UT)	Interferometer Configuration[a]	Calibrator Names (Adopted UD Diameter)
	$\lambda\ Vir$ (A1V + A); H mag = 4.28±0.21	
2003 Feb 16,17	A35-B05-C10	HD 126035 (G7III, 0.78±0.24 mas, getCal[b])
		HIP 71957 (F2III, 1.20±0.22 mas, getCal)
2003 Feb 20,22,23	A25-B15-C10	HD 126035
2003 Mar 21	A35-B07-C25	HD 126035
2003 Mar 22	A35-B07-C10	HD 126035; HD 158352 (A8V, 0.44±0.10, getCal)
2003 Mar 23-24	A35-B15-C10	HD 126035; HD 158352
2003 Jun 12-17	A35-B15-C10	HD 126035
	WR 140 (WC7 + O4/5); H mag = 5.429±0.023	
2003 Jun 17	A35-B15-C10	HD 192985 (F5IV, 0.46±0.10 mas, getCal)
		HD 193631 (K0, 0.44±0.10 mas, getCal)

*Note: H-band photometry from 2MASS All-Sky Release

[a]Configuration refers to the location of telescopes A,B,C on the NE, SE and NE arm respectively; see §2 for more details

[b]*getCal* is maintained and distributed by the Michelson Science Center (http://msc.caltech.edu)

Table 2. Binary Parameters for λ Vir and WR 140 at 1.65μm

Source	Epoch (U.T.)	Separation (milliarcseconds)	Position Angle[(a)] (degrees)	Flux Ratio	χ^2/DOF[(b)] V^2	CP
λ Vir	2003Feb16-23	18.2 ± 0.6	200 ± 3	$1.69^{+0.29}_{-0.21}$	0.45	12.8
	2003Mar21-24	17.8 ± 0.5	184 ± 3	1.72 ± 0.07	0.33	2.2
	2003Jun12-17	19.5 ± 0.6	22 ± 3	$2.05^{+0.50}_{-0.35}$	0.31	4.8
WR 140	2003Jun17	$12.9^{+0.5}_{-0.4}$	$151.7^{+1.8}_{-1.3}$	$1.10^{+0.06}_{-0.05}$	0.13	4.7

*Note: Reported binary parameters are the most probable values with 1-sigma errors bars (68.4% confidence interval)

[a]Since component masses are not definitively known yet, position angles (East of North) are measured from the bright to the faint component.

[b]The χ^2 per DOF (degree of freedom), the *reduced* χ^2, is reported for the model fit to the $\mathcal{V}^2$and closure phases (CP) measurements separately.

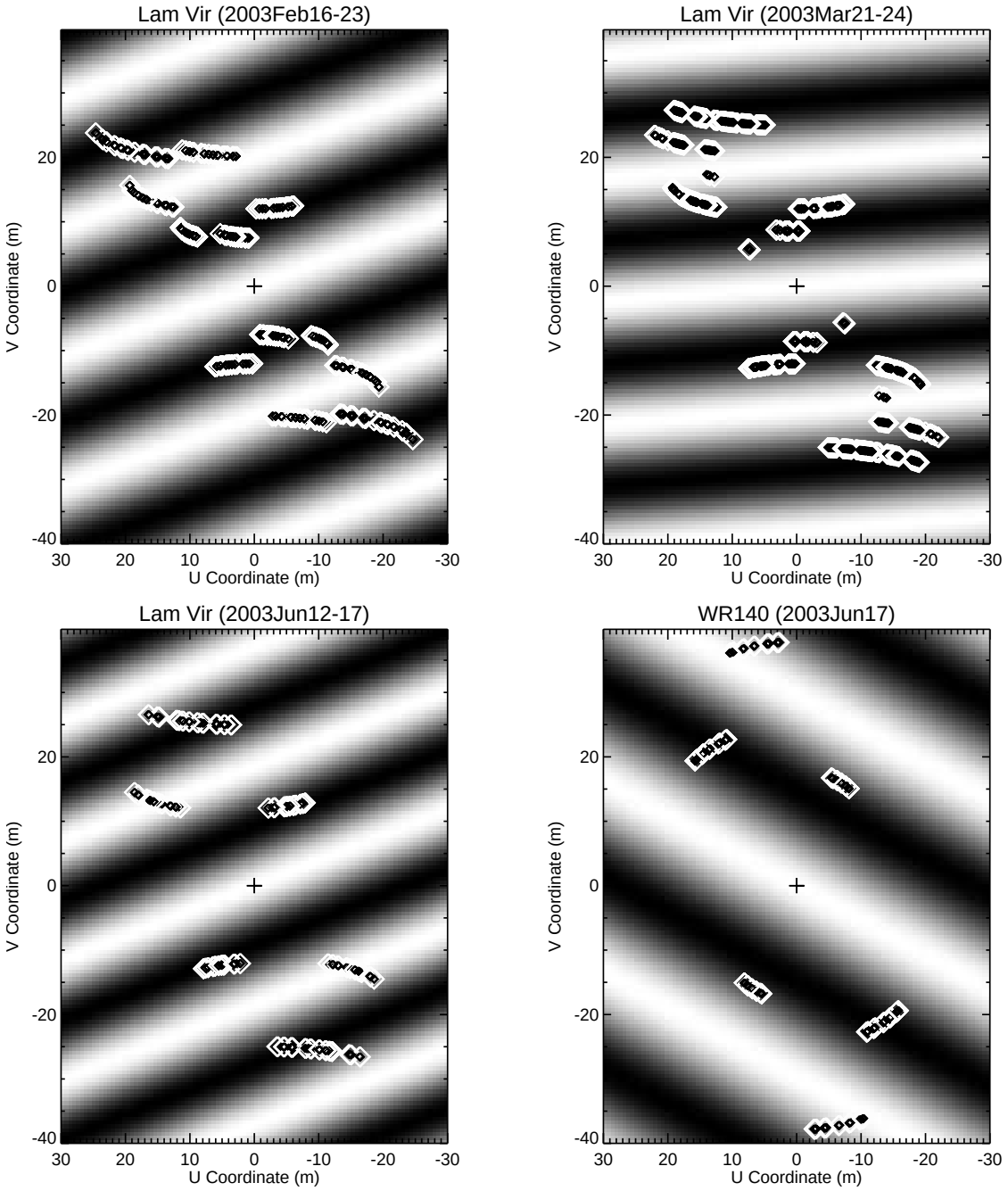

Fig. 1.— (u,v)-plane coverage of science binaries. Each diamond symbol represents a single observation with the IOTA3 interferometer, corresponding to approximately 100-200 interferogram scans. The overlaid image in each panel represents the $\mathcal{V}^2$of the best fit binary model for each epoch discussed in text.

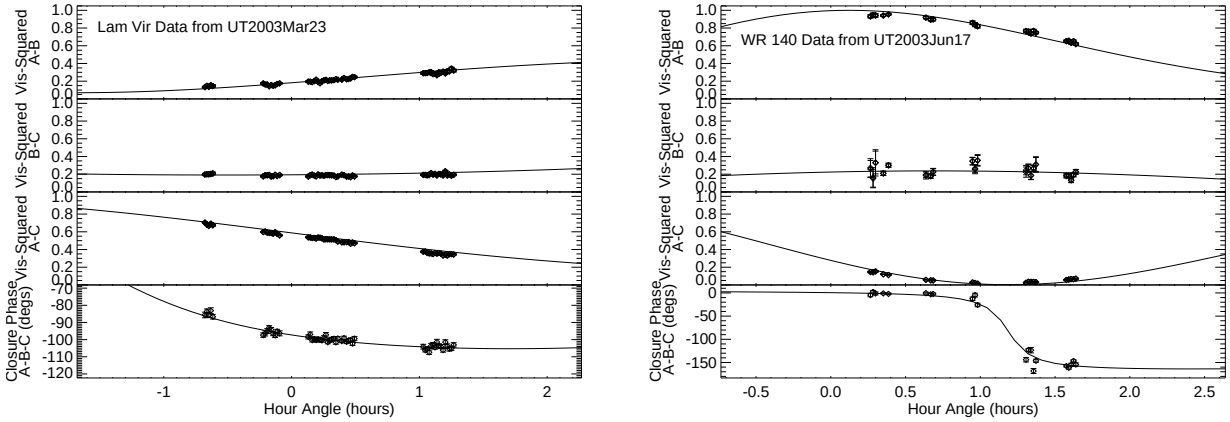

Fig. 2.— *(left panel):* This figure shows example binary model fits for λ Vir on UT2003Mar23. The top three panels show the $\mathcal{V}^2$for baselines connecting telescopes A-B, B-C, and A-C, respectively. The bottom panel shows the calibrated closure phase for the A-B-C triangle. *(right panel):* Same as left panel for UT2003Jun17 observations of WR 140. These curves represent the best-fit model parameters (as described in §4) For all panels, the error bars shown represent only the statistical error and do not include the systematic error discussed in the text (§3). Refer to Table 2 for estimate of the binary parameters.

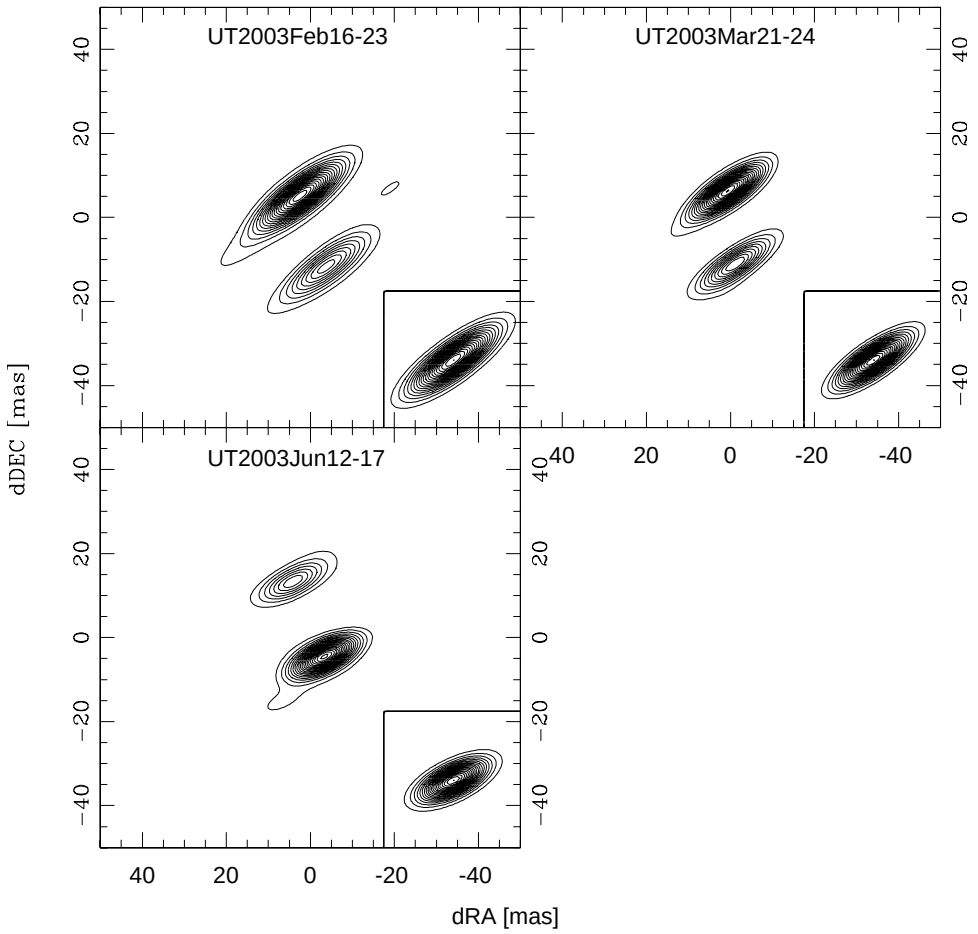

Fig. 3.— First aperture synthesis images from the upgraded IOTA 3-telescope interferometer, depicting λ Vir based on 1.65μm observations at three separate epochs. The binary components are well-resolved from each other but individually are unresolved; orbital motion is clearly evident between the epochs. North is up and East is left in this contour map using 5% intervals in surface brightness scaled to the peak in each map. The CLEAN restoring beam is depicted in the lower-right corner of the panel.